

Splitting failure mode of bonded anchors

T. Hüer & R. Eligehausen

Institute of Construction Materials, University of Stuttgart, Stuttgart, Germany

ABSTRACT: Different fastening systems are available nowadays to transfer any given load combination into a concrete member. Bonded anchors are one of the most commonly-used systems. Their failure under tensile loading occurs in two different ways, following the formation of either a conical crack or a number of splitting cracks. In this paper, the attention is focused on the latter failure mode, that may occur with fastenings located close to an edge or to a corner, particularly when the thickness of the member is small. The objective is to define a suitable design approach for bonded fastenings characterized by a splitting-type failure. To this end, numerical and experimental studies were carried out, the former being based on nonlinear finite-element modelling. The results are presented and discussed in this paper, together with the proposal of the aforementioned design approach. Finally, the analogy between the proposed approach and that adopted in the design of lap splices in R/C members is discussed.

1 INTRODUCTION

Fastenings are used to transfer loads, e.g. from steel constructions, in concrete members. Adhesive bonded anchors are a popular fastening system. They consist of an injection mortar or a resin capsule and a threaded rod. In case of tensile loading of bonded anchors, failure of the concrete takes place as a concrete cone breakout or, similar to reinforcing bars, by generating of splitting cracks (Eligehausen et al. 2006). A failure due to splitting cracks may occur with fastenings located near to an edge or a corner, especially in a thin member.

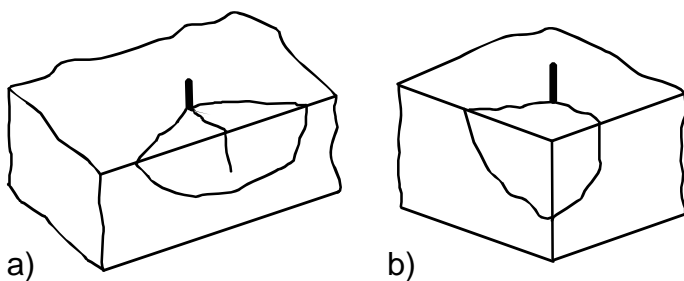


Figure 1. Splitting failure of a single anchor a) close to an edge and b) in the corner.

Splitting failure is caused by splitting forces, which are generated in the concrete member by tensile loaded fasteners (Asmus 1999). The splitting force generates cracks growing from the anchor to the

edge and consequently the edge of the member spalls (Fig. 1).

Due to the load transfer of bonded anchors, compressive stresses occur in the concrete bordering the load bearing area of an anchor. This pressure generates tensile hoop stresses. These tensile stresses act like splitting forces. The splitting forces increase with the tension load.

The ultimate load at splitting failure of an anchorage is affected by the material properties of the concrete and of the mortar. As well the ultimate load depends on the size of the activated fracture surface. The size of the fracture surface is determined by geometric conditions like distances to the edges of the member, the member thickness and the anchor spacing in groups. Furthermore, the geometrical parameters of the anchor (diameter and embedment depth) influence its capacity.

Up to now a design concept to predict the splitting failure load is not available. With the view to develop such a design concept numerous numerical simulations and experimental tests were performed. The design approach is based on the results of the numerical investigations and validated by experimental tests.

All investigations were performed as confined tests. In confined tests concrete cone failure is eliminated by transferring the reaction force close to the anchor into the concrete. Furthermore, no bending stresses are generated. This test set-up was chosen for the investigations for two reasons: first no mix-

ture of splitting failure and concrete cone breakout will occur and second no bending stresses are generated, which would superpose with the stresses generated by the splitting forces.

2 THE PROPOSED DESIGN CONCEPT

The proposed design concept for the splitting failure mode of bonded anchors provides to calculate initially a base value of a single anchor at the edge (Equation 1). All the geometrical parameters, which influence the base value, are shown in Figure 2. For the base value the characteristic member thickness $h_{cr,sp}$ is assumed. At this thickness the member provides the maximum capacity and a reduction of the member thickness induces a decrease of the capacity. Further on, the base value depends on a product factor k_p , the size of the load bearing area (anchor diameter d and embedment depths h_{ef}), the edge distance c_1 and the concrete compressive strength f_{cc} . The product factor has to be evaluated by tests.

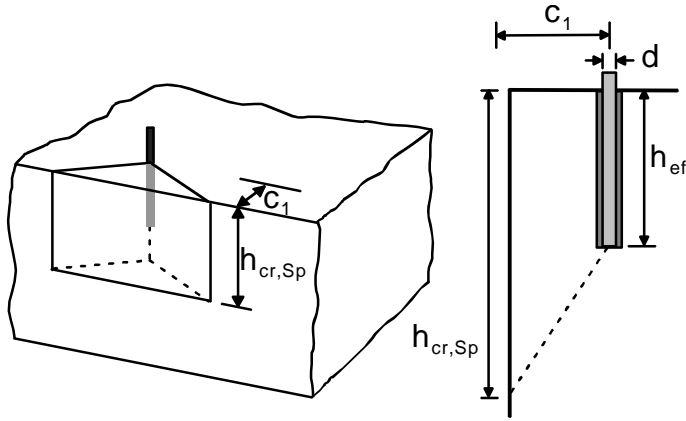


Figure 2. Geometrical parameters.

$$N_{u,sp}^0 = k_p \cdot (\pi \cdot d \cdot h_{ef})^{1/2} \cdot c_1^{3/7} \cdot h_{cr,sp}^{1/6} \cdot f_{cc}^{1/2} \quad [\text{N}] \quad (1)$$

with

$$h_{cr,sp} = 1.5 \cdot c_1 + h_{ef} \quad [\text{mm}]$$

The approach assumes that the resistance of the concrete to splitting forces is proportional to the concrete tensile strength. According to Eligehausen et al. (2006) the concrete tensile strength corresponds with sufficient accuracy throughout the whole range of concrete compressive strengths to the square root of the compression strength.

In case of the design of an actual application, e.g. an anchors group close to an edge or an anchor in the corner of the member, the corresponding fracture surface is projected onto the edge of the member. The failure load of the application is given by Equation 2.

$$N_{u,sp} = \frac{A_{c,sp}}{A_{c,sp}^0} \cdot \Psi_{h,sp} \cdot \Psi_{g,sp} \cdot N_{u,sp}^0 \quad [\text{N}] \quad (2)$$

with

$$\Psi_{h,sp} = \left(\frac{h_{cr,sp}}{h} \right)^{5/6}$$

$$s_{cr,sp} = 5 \cdot c_1^{2/3} \cdot d^{1/3} \leq 32 \cdot d \quad [\text{mm}]$$

$$\Psi_{g,sp} = \sqrt{n} - (\sqrt{n} - 1) \cdot \sqrt{\frac{s}{s_{cr,sp}}} \geq 1$$

$$A_{c,sp}^0 = s_{cr,sp} \cdot h_{cr,sp}$$

$A_{c,sp} / A_{c,sp}^0$ is the ratio of the projected area of the application to the projected area of the single anchor at an edge. $N_{u,sp}^0$ is the base value from Equation 1. The factor $\Psi_{h,sp}$ ensures that the actual member thickness h is considered with the same power as the characteristic member thickness in Equation 1. At calculating Equation 2 the actual member thickness is limited to the characteristic member thickness.

In case of anchor groups where n is the number of anchors the factor $\Psi_{g,sp}$ considers the larger load bearing area in comparison to a single anchor. The factor $\Psi_{g,sp}$ starts with a value of square root n for an anchor spacing of zero and declines to one for an anchor spacing equal to the characteristic anchor spacing. The characteristic anchor spacing $s_{cr,sp}$, where the anchors do not affect each other, depends on the edge distance and on the diameter of the threaded rod.

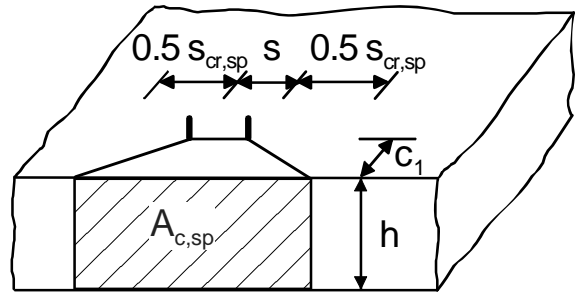


Figure 3. Projected area of a group of two anchors.

Figure 3 shows the example of a group of two anchors with the spacing s located close to an edge. The projected area of this application is:

$$A_{c,sp} = (s_{cr,sp} + s) \cdot h \quad (3)$$

The proposed design approach is primarily based on the results of the numerical study, that is presented in the next chapter. In addition to the results of the

simulations the corresponding curves of the design approach are plotted in the figures of chapter 3.

3 NUMERICAL INVESTIGATIONS

3.1 Finite element code

In the following numerical study the finite-element (FE) code MASA was used. This program, developed by Ožbolt, is intended for the nonlinear two- and three-dimensional analysis of structures made of quasi-brittle materials such as concrete. It is based on the microplane model (Ožbolt et al. 2001), a macroscopic material model, and a smeared crack approach.

In the microplane model the material is characterized by an uniaxial relation between the stress and strain components on planes of various orientations. At each integration point these planes may be imagined to represent the damage planes or weak planes of the microstructure. The tensorial invariance restrictions need not be directly enforced. Superimposing the responses from all microplanes in a suitable manner automatically satisfies them.

In the analysis of materials which exhibit fracture and damage phenomena, such as concrete, one has to use a so-called localization limiter to assure mesh independent results. In the program MASA two approaches can be used: a crack band approach and a more general nonlocal approach of integral type. In the present study the crack band approach was employed. In the approach the constitutive law is related to the element size such that the specific energy consumption capacity of concrete is independent of the size of the finite element.

3.2 The finite element model

All constituents of the model were discretized by four-node tetrahedra elements. The mesh was refined within the area of the bonded anchor. To limit the element number only every second thread of the threaded rod was modeled and the geometry of the thread was simplified (Fig. 4b). The behavior of steel was assumed to be linear elastic with a Young's modulus $E_S = 205000$ MPa and a Poisson's ratio $\nu_S = 0.3$. The diameter of the threaded rod was varied.

The steel elements of the threaded rod are connected and interlocked with the elements of the mortar layer. The mortar layer was simulated using microplane parameters which are adjusted to the mechanical properties of an actual product. The Young's modulus amounts to $E_B = 5700$ MPa and the Poisson's ratio to $\nu_S = 0.25$. The mortar elements are coupled with the concrete elements. The material properties of the concrete are: Young's modulus $E_S = 205000$ MPa, Poisson ratio $\nu_S = 0.18$, tensile

strength $f_t = 2.2$ MPa and uniaxial compressive strength $f_c = 28$ MPa.

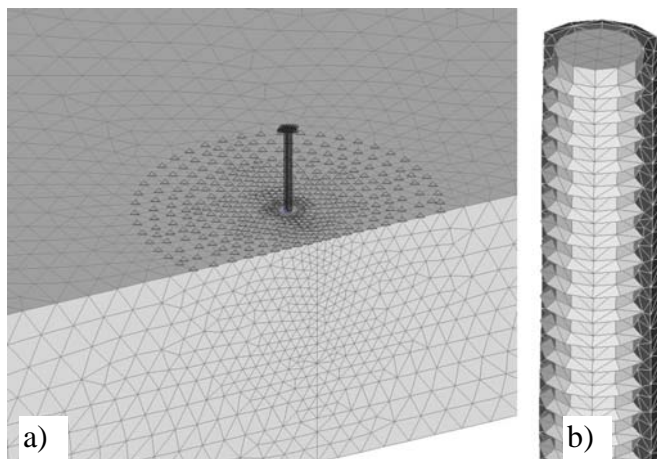


Figure 4. FE model: a) mesh of the concrete member and b) threaded rod with mortar layer.

To simulate a confined test set-up all nodes of the concrete elements at the upper surface within a radius of 1.5 times the embedment depth were fixed in load direction (Fig. 4a). The tensile load was applied by incremental displacements of the threaded rod.

3.3 FE simulations compared with design method

Figure 5 shows the numerically obtained principal strains of a single anchor close to an edge at ultimate load. The dark regions display areas of damage or cracking. The crack pattern agrees well with the crack pattern observed in tests.

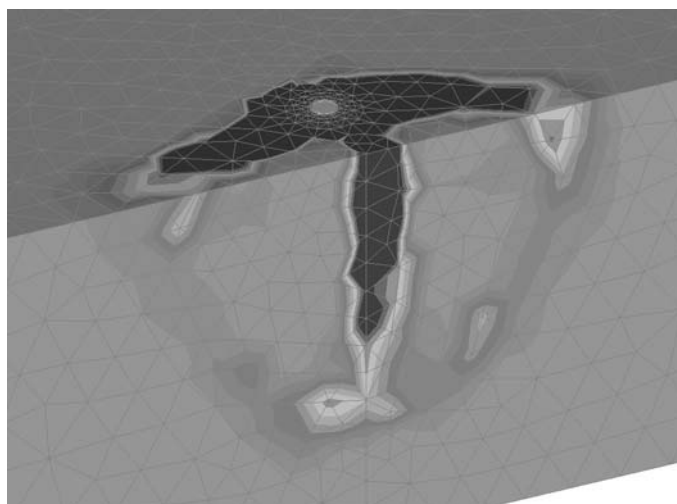


Figure 5. Crack pattern of FE simulation, single anchor near an edge, small edge distance.

Before reaching the peak load a crack begin to form perpendicularly from the edge to the anchor. At peak load at both sides of the anchor cracks grow transversal to the edge. Figure 6 shows the crack formation of an anchor with a larger edge distance than in Figure 5. From Figure 6 can be seen that the average measured angle between edge and splitting crack is larger for the larger edge distance. That means the

angle grows up with the edge distance and consequently the increase of the fracture surface is not proportional to the edge distance.

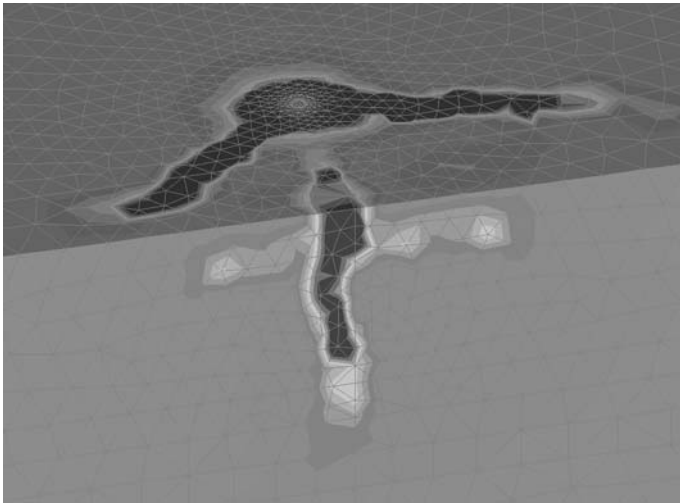


Figure 6. Crack pattern of FE simulation, single anchor at the edge, large edge distance.

Initially, numerical simulations with a single anchor close to the edge were performed. The anchor diameter (12 mm) and the embedment depth (120 mm) were kept constant. The edge distance was varied. In Figure 7 the numerically obtained failure loads are plotted as a function of the edge distance for two different concrete member thicknesses. At small edge distances no influence of the member thickness on the ultimate load can be recognized. With increasing edge distance, however, the thick concrete member provides a larger increase in ultimate load than the thin member.

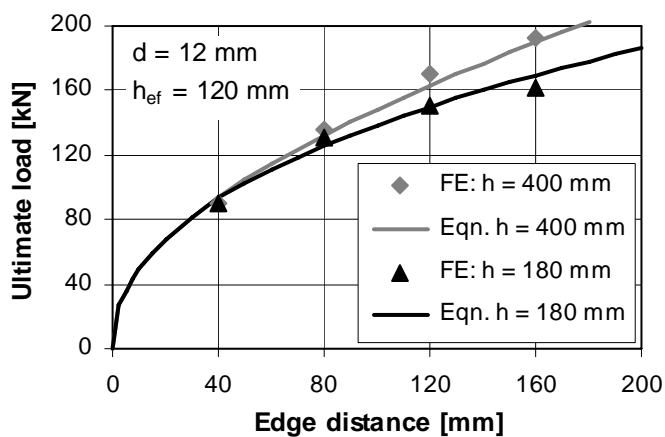


Figure 7. Influence of the edge distance.

To investigate the influence of the concrete member thickness more precisely, numerical calculations with different member thicknesses were performed for two different edge distances. Figure 8 displays failure loads of the simulations plotted against the member thickness. For a small edge distance of 80 mm the maximum load of this edge distance is obtained at a member thickness of about 230 mm.

However, for the greater edge distance (160 mm) the load increase up to a member thickness of about 350 mm. Thus, the member thickness that provides the maximum capacity increase with the edge distance.

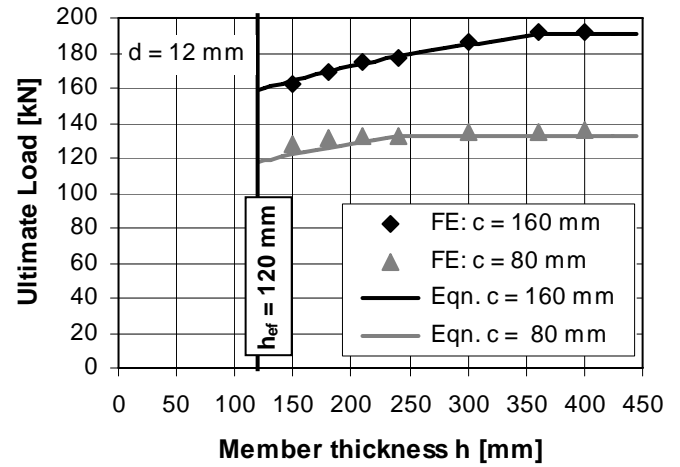


Figure 8. Influence of the member thickness.

Figure 9 shows the numerically obtained ultimate load as a function of the embedment depth related to the anchor size. The edge distance of the simulations was kept constant (160 mm). Two anchor sizes were examined. The member thickness of the simulations with the anchor size 12 mm corresponded to the characteristic member thickness. For the anchor size 24 mm the member thickness was 120 mm larger than the embedment depth.

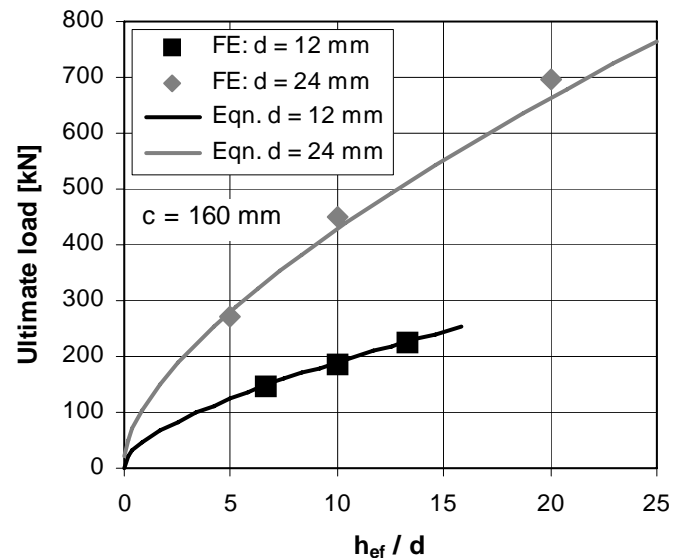


Figure 9. Influence of the embedment depth.

Figure 10 illustrates the numerically obtained splitting load of a group of two anchors near an edge (Fig. 3) as a function of the anchor spacing. While the anchor size (12 mm) and the embedment depth (120 mm) were kept constant, four different edge distances were investigated. The failure load increases with increasing spacing until it reaches a

limit of n-times the capacity of a single anchor. The corresponding anchor spacing $s_{cr,sp}$ increases with the edge distance. For the smallest edge distance the double load of the single anchor is obtained by an anchor spacing of about 150 mm, whereas for the large edge distance of 160 mm an anchor spacing of more than 300 mm is necessary.

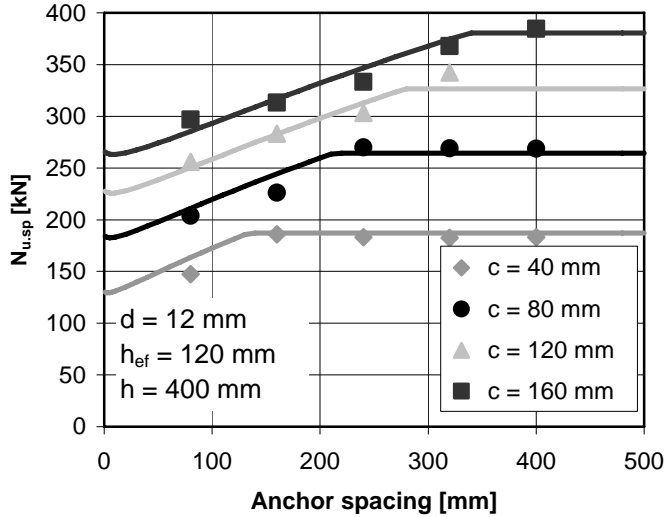


Figure 10. Anchor group at the edge, different edge distances.

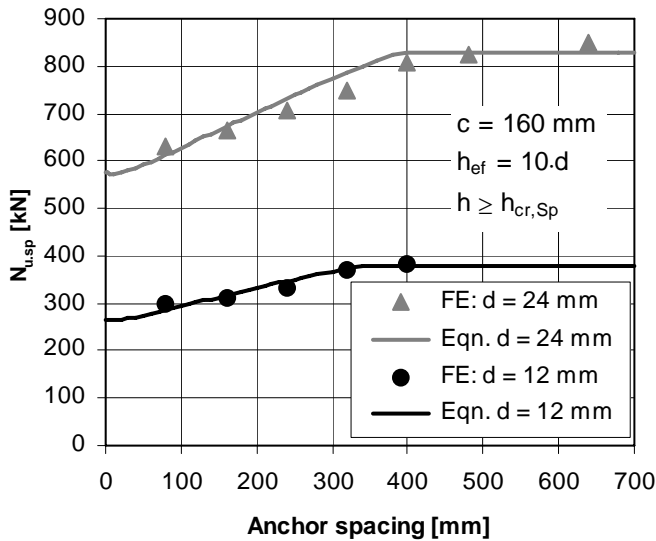


Figure 11. Anchor group at an edge, different anchor sizes.

Further on, FE simulations with an anchor group of the anchor size 24 mm were performed. The edge distance was kept constant. The results are shown in figure 11. The failure loads of the anchor size 12 mm and an edge distance of 160 mm of figure 10 are also plotted in figure 11. For the anchor size 24 mm an increase of the spacing from 320 to 400 mm leads obviously to an increase of the failure load. However, in case of an anchor size of 12 mm the loads of these two anchor spacings show almost no difference. That means the n-times load of a single anchor is obtained at a smaller spacing for the anchor size 12 mm than for the anchor size 24 mm.

It can be summarized that the characteristic anchor spacing $s_{cr,sp}$ depends on the edge distance (Fig. 10) as well as on the anchor size (Fig. 11).

4 EXPERIMENTAL TESTS

The tests on single anchors close to an edge were carried out for four different adhesive anchoring systems. The systems differ in their chemical composition. That induces different mechanical properties, e.g. bond strength. The edge distance, anchor size, embedment depth and member thickness was varied. Figures 12 to 15 show the ratio of measured failure load and the load calculated in accordance with Equation 2 as a function of the anchor size (Fig. 12), the embedment depth (Fig. 13), the edge distance (Fig. 14) and the member thickness normalized by the characteristic member thickness (Fig. 15). The respective product factor was identified from the mean value of a series with an edge distance of 40 mm, an anchor size of 12 mm and an embedment depth of 70 mm. The particular product factors are given in Table 1. The product factors of the mortars B to D have a similar value. The factor of product A is about 50% larger. System A represents an epoxy resin, which provides generally larger bond strength than the other adhesive systems.

Table 1. Product factors.

Product	Product factor
A	24.0
B	16.4
C	16.8
D	16.2

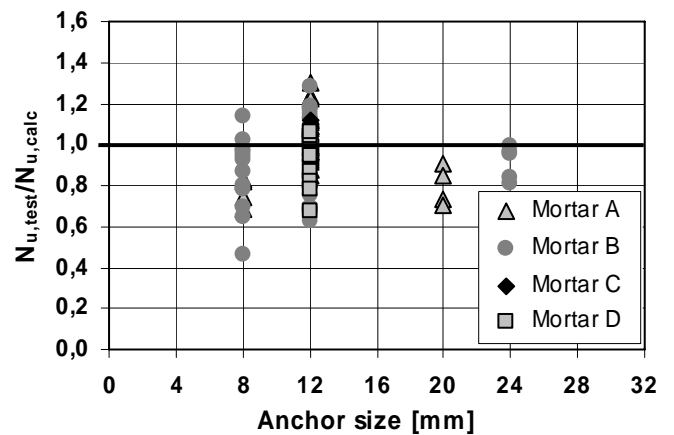


Figure 12. Ratio test to design load against anchor size.

Figure 12 illustrates the ratios test load $N_{u,test}$ to design load $N_{u,calc}$ plotted against the anchor size. The ratios $N_{u,test}/N_{u,calc}$ are located at 1.0. That means the failure load is well taken into account by the proposed design approach.

The mean value of $N_{u,test}/N_{u,calc}$ of the 115 tests is 0.95 and the coefficient of variation is 16.3%. There are no noticeable tendencies in the diagrams (Fig. 12)

to Fig. 15) which would indicate that one of the parameters is considered in a wrong way. Overall the design concept shows a rather good representation to the test data.

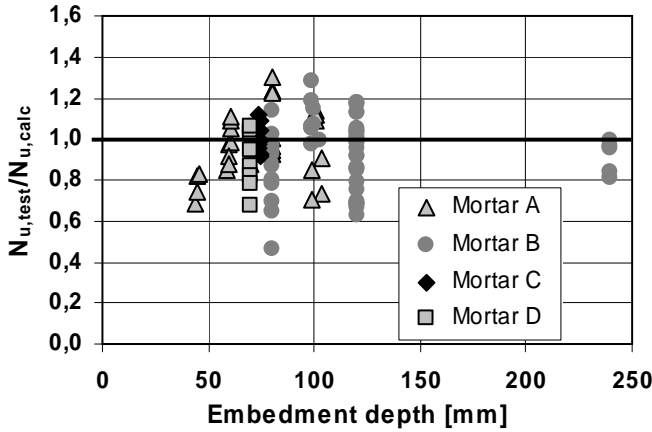


Figure 13. Ratio test to design load against embedment depth.

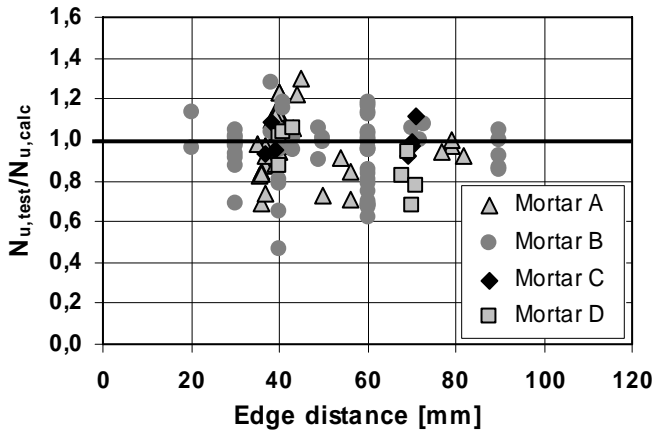


Figure 14. Ratio test to design load against edge distance.

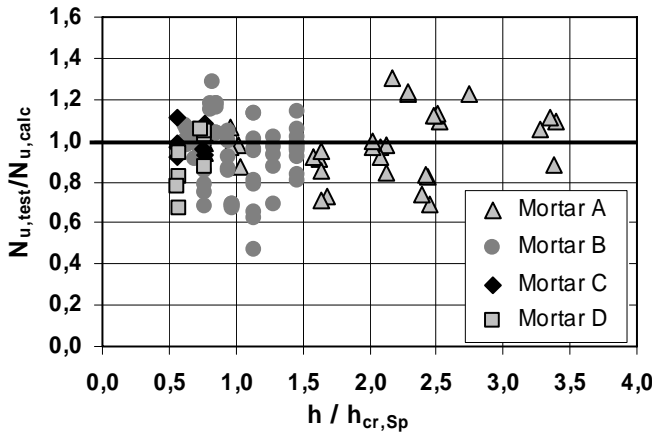


Figure 15. Ratio test to design load against member thickness.

5 COMPARISON WITH REINFORCING BARS

5.1 Splitting failure of reinforcing bars

The failure of lap splices and anchorages of rebars occur typically by splitting or blasting of the concrete. Eligehausen (1979) developed a design concept to predict the ultimate steel stress of rebars at splitting failure of lap splices. He distinguishes between different failure modes.

The failure mode C (Fig. 16) occurs, if the fracture is not affected by a further edge or an adjacent lap splice. The crack pattern is similar to a single (bonded) anchor close to an edge. In the following the design concept of Eligehausen for failure mode C (Rebar) is compared with the proposed design approach for bonded anchors (BA).

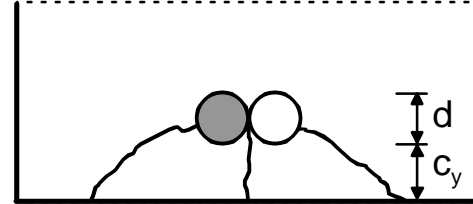


Figure 16. Failure mode C of lap spliced reinforcing bars.

According to Eligehausen the following parameters have a decisive influence on the failure load: the concrete cover c_y , the bar diameter d , the length of the lap splice h_{ef} and the concrete compressive f_{cc} strength. The member thickness has no influence, since it is for lap splices in principle larger than the characteristic member thickness.

5.2 Comparison of the design concepts

Eligehausen (1979) indicates two different equations to calculate the ultimate steel stress of rebars at splitting failure: one associated with a concrete cover smaller than $2.5d$ and one for a concrete cover larger than $2.5d$. Transforming the equations from stress to load leads to the following equations:

$$N_{u,sp} = 7.66 \cdot c_y^{1/2} \cdot h_{ef}^{2/3} \cdot d^{5/6} \cdot f_{cc}^{1/2} \cdot K \quad [\text{N}] \quad (3a)$$

for $c_y \leq 2.5 \cdot d$

$$N_{u,sp} = 9.64 \cdot c_y^{1/4} \cdot h_{ef}^{2/3} \cdot d^{13/12} \cdot f_{cc}^{1/2} \cdot K \quad [\text{N}] \quad (3b)$$

for $c_y > 2.5 \cdot d$

$$\text{with } K = 1.2 \cdot k_d \text{ and } 0.75 \leq k_d = \left(\frac{10}{d} \right)^{1/2} \leq 1.10$$

The comparison of the two design concepts shall disclose potential differences in the influence of the parameters on the failure load. Therefore, the curves of the equations of the two models are plotted together in the Figures 17 to 19. The product factor of

the proposed design model was set to 12, since that leads to similar ultimate loads of the both models.

For the comparison relative to the edge distance the diameters 12 and 24 mm were chosen. Figure 17 displays the ultimate loads of both design concepts as a function of the edge distance related to the rod/bar diameter. Since the concrete cover is a half bar diameter smaller than the edge distance, the curve of the rebar starts at an edge distance of a half bar diameter.

Up to an edge distance of $3d$ the increase of the ultimate load of the lap splices is larger than of the bonded anchors. In contrast, for larger edge distances the increase is smaller. For the design of bonded anchors the range $2d$ to $6d$ is important: at smaller edge distances no installation is possible and at larger edge distances than $6d$ a pull out failure takes place normally. In the range mentioned before the values of both design concepts are similar for the observed diameters.

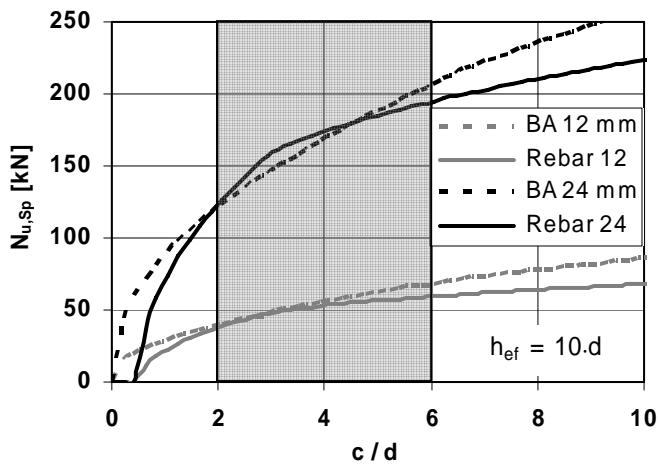


Figure 17. Influence of the edge distance.

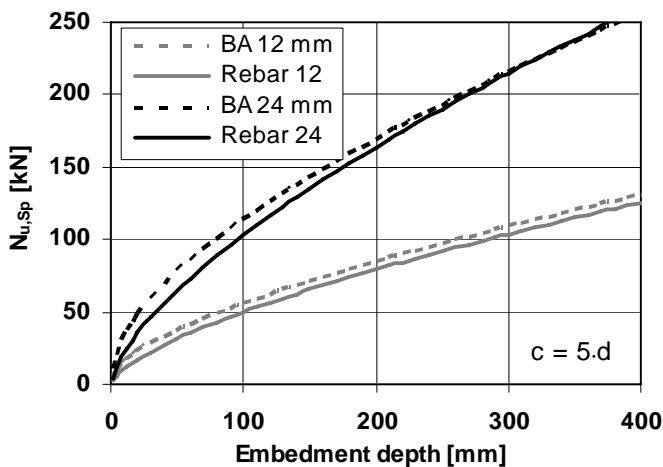


Figure 18. Influence of the embedment depth. Figure 18 presents that the increase of the splitting failure load with the embedment depth is very similar for both design concepts. This is valid for both observed diameters. The underlying edge distance is the quintuple rod or bar diameter.

For a comparison of the influence of the bar and rod diameter, respectively, two different edge distances were chosen: 60 and 120 mm. In Figure 19 the splitting failure load is plotted against the diameter. For the diameters 8 to 18 the increase of both models is very similar. However, for diameters larger than 18 the design concept of Eligehausen show a greater slope than the proposed design approach.

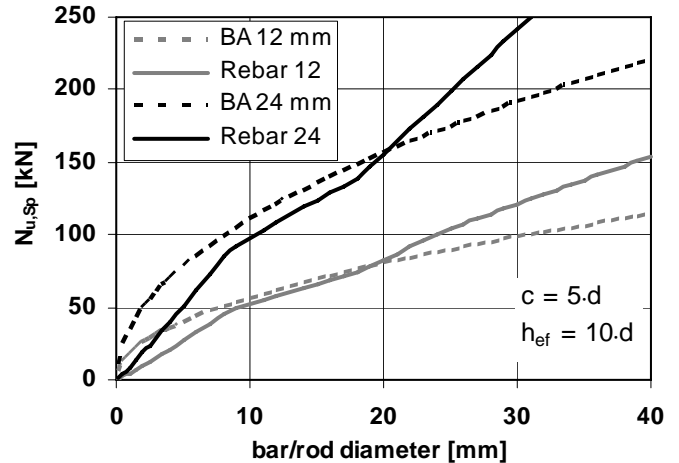


Figure 19. Influence of the bar/rod diameter.

The influence of the concrete strength is equal for both design concepts. In both concepts the concrete compressive strength is considered with a power of $1/2$. Overall the influence of the edge distance, the embedment depth and the concrete compressive strength is considered by both design concepts in a similar way. A noteworthy difference between the compared concepts can be observed only for the influence of the diameter.

6 CONCLUSIONS

Bonded anchors subjected to tensile loads often fail by concrete splitting. To understand to what extent the ultimate capacity is affected by the many geometric and mechanical parameters controlling splitting failure, numerous FE simulations were carried out, in order to develop a new semi-empirical design approach. This approach is presented here, together with the results of the numerical simulations.

According to the proposed approach, the ultimate capacity of a single anchor close to an edge is worked out and is considered as a “base” value. The capacity of an arbitrary anchorage can be evaluated by means of projected areas. Therefore, the failure surfaces are projected on the edge of the concrete member.

As a rule, there is a satisfactory agreement between the proposed design approach (that was validated through specific tests carried out by the authors) and the numerical results.

Furthermore, comparing the proposed approach with that used in the design of lap splices shows that in both anchors and spliced bars splitting failure is governed by the same parameters.

Summing up, the proposed design approach is a useful and realistic tool to predict the ultimate capacity of bonded anchors failing because of concrete splitting.

REFERENCES

- Asmus, J. 1999. *Bemessung von zugbeanspruchten Befestigungen bei der Versagensart Spalten des Betons (Design of tensile loaded anchorages at concrete splitting)*. Doctor thesis, University of Stuttgart.
- Eligehausen, R. 1979. *Übergreifungsstöße zugbeanspruchter Rippenstäbe (Lapped splices of tensioned rebars)*. Berlin: Schriftenreihe DAfStB, No. 301.
- Eligehausen, R., Mallee, R. & Silva, J.F. 2006. *Anchorage in Concrete Construction*. Berlin: Ernst & Sohn Verlag für Architektur und technische Wissenschaften GmbH.
- Ožbolt, J.; Li, Y.-J.; Kožar, I. 2001: *Microplane model for concrete with relaxed kinematic constraint*. International Journal of Solids and Structures. 38: 2683-2711.